Computational Fluid Dynamics Simulation of Regime Transition in Bubble Columns Incorporating the Dual-Bubble-Size Model

Jianhua Chen,[†,‡] Ning Yang,*[,†] Wei Ge,[†] and Jinghai Li[†]

State Key Laboratory of Multi-Phase Complex System, Institute of Process Engineering, Chinese Academy of Sciences, P.O. Box 353, Beijing, 100190, P.R. China, and Graduate University of Chinese Academy of Sciences, Beijing 100049, P.R. China

This article investigates the two regime transition points for bubble columns with the so-called dual-bubble-size (DBS) model featuring the utilization of a stability condition to analyze the compromise between dominant mechanisms. Our previous work indicated that the second point could be reasonably predicted and physically interpreted by the DBS model for various gas−liquid systems. This work further clarifies the relationship between the bifurcation of energy dissipation and of structural parameters and the regime transition. It is found that the bifurcation of energy dissipation exists for both the gas−liquid and gas−solid systems and can be used to predict and understand regime transition in multiphase flow. Then the DBS model is incorporated into the two-fluid model for calculating interphase coupling, and a computational fluid dynamics (CFD) calculation is performed to simulate a bubble column. The "shoulder" on the gas hold-up curve can be observed in the simulation with the new coupling method, and the second transition point predicted from the CFD simulation is consistent with experiments and the calculation of the DBS model. Sparger effects are investigated through the two simulation cases for uniform aeration and local aeration, and the radial distribution of local hydrodynamic parameters is comparable with experimental data in the literature.

1. Introduction

Bubble columns are widely utilized in chemical, petrochemical, biochemical, and pharmaceutical industries. But their multiscale flow structures and versatile hydrodynamic regimes complicate the understanding of interphase momentum and mass transfer and hence the design and scale-up of bubble column reactors.[1] Three flow regimes have been found to exist in bubble columns:[2] the homogeneous regime occurs at lower gas velocities, followed by a transition regime at intermediate gas velocities, and finally the heterogeneous regime appears at higher gas velocities. Regime transition can be identified via the variation of gas hold-up with superficial gas velocity. Zahradnik et al.[2] found two transition points for air−water systems with perforated spargers. The first was recognized by the slope change at 0.04 m/s of gas velocity, reflecting the deviation from homogeneous regime. The second was characterized by a local minimum of gas hold-up at 0.125 m/s of gas velocity, indicating the regime transition into a fully developed heterogeneous regime. Within the curve between these two points is the so-called "transition regime" known as a flow pattern with complicated coherent structures.[3] The curve of gas hold-up may take on a shoulder- or a plateaulike shape, depending on operating conditions and sparger types.[4] For nonuniform aeration, Ruzicka et al.[5] reported that gas hold-up increases monotonously within the whole range of gas velocity and no shoulder or plateau can be observed, but this hold-up curve rejoins with that for the uniform aeration case at higher gas velocities. For many other aeration methods which lie between the uniform and nonuniform cases, the second transition point may reflect some fundamental structure transformation. However, to our knowledge, most modeling studies on regime transition, like the drift flux model[6] and linear stability analysis,[7] focus generally on the first transition point, and few models can theoretically predict or interpret the second transition point.

Computational fluid dynamics (CFD) has been emerging as a powerful tool for cognizing the flow behavior in bubble columns in recent decades. It is reported that the unresolved issues for CFD modeling involve the model formulation for multiphase turbulence, bubble coalescence, and breakup, especially the interphase momentum transfer. Regime transition is still far less investigated with CFD study. Krishna et al.[8] utilized a three-fluid model by considering the liquid, "small" bubble and "large" bubble as separate interpenetrating phases, and the first transition point was designated before simulation. Olmos et al.[9] tried to predict the two transition points by using a multiple gas phase Euler−Euler model, concluding that it was unable to predict transition points when only one single gas phase was considered. Monahan et al.[10] investigated the effects of grid resolution and force models in the two-fluid model and simulated transitional flow regime at intermediate gas velocities based on the observation of the water volume fraction profiles. The transition to churn-turbulent flow (heterogeneous regime) was not observed, which was attributed to the neglect of bubble coalescence. Wang et al.[11] coupled the two-fluid model, and a population balance equation to predict the first transition point characterized by a sharp decrease in small bubbles volume fraction. Simonnet et al.[12] discussed the influence of correction function for local volume fraction upon drag coefficient and proposed a drag correlation which could reproduce the shoulder- or plateaulike shape of global gas hold-up as a function of superficial gas velocity.

Our recent work[13,14] indicates that the so-called dual-bubble-size (DBS) model could capture the two regime transition points on the curve of gas hold-up vs gas velocity and the calculation is consistent with the experiments of Camarasa et al.[4] and Zahradnik et al.[2] Moreover, this model could offer some physical explanation on regime transition through the analysis of energy dissipation at different scales. The dual effects of liquid viscosity and surface tension were reasonably predicted. This work further

* To whom correspondence should be addressed. E-mail: nyang@home.ipe.ac.cn. Tel.: +86-10-82627076. Fax: +86-10-62558065.
[†] Chinese Academy of Sciences.
[‡] Graduate University of Chinese Academy of Sciences.

10.1021/ie801644d CCC: $40.75
Published on Web 05/21/2009

elucidates the essential relationship between regime transition and bifurcation of structural parameters for gas−liquid and gas−solid systems respectively, and some common characteristics of these two systems are investigated. Then, a novel drag model is proposed based on the DBS model established previously which, we believe, can not only describe the global structure variation of system but also reflect the hydrodynamic interaction between phases. With this new drag model, a CFD simulation is implemented and compared with experimental data in literature. It is interesting to see that CFD simulation with this model can obtain the "shoulder" on the gas hold-up curve, though quantitative agreement of local behavior with experiments is not fully achieved partly due to the simplified treatment of sparger types in 2D simulation.

2. Relationship between Structural Bifurcation and Energy Dissipation

In the DBS model established in our previous work,[13] the global gas−liquid system is simply resolved into one liquid phase and two bubble classes depicted by six structural parameters, i.e, bubble diameters (d_S, d_L), volume fraction (f_S, f_L), and superficial gas velocities ($U_{g,S}$, $U_{g,L}$). The liquid structure is assumed to be shared between the two bubble classes and therefore not resolved. Then, the following conservation equations can be formulated. The mass conservation equation can be written as

$$U_{g,S} + U_{g,L} = U_g \tag{1}$$

A force balance leads to two conservation equations separately for the two bubble classes:

$$f_S \rho_l g = \frac{f_S}{\pi/6 \cdot {d_S}^3} \cdot C_{D,S} \frac{\pi}{4} {d_S}^2 \cdot \frac{1}{2} \rho_l \left(\frac{U_{g,S}}{f_S} - \frac{U_l}{1 - f_b} \right)^2 \tag{2}$$

$$f_L \rho_l g = \frac{f_L}{\pi/6 \cdot {d_L}^3} \cdot C_{D,L} \frac{\pi}{4} {d_L}^2 \cdot \frac{1}{2} \rho_l \left(\frac{U_{g,L}}{f_L} - \frac{U_l}{1 - f_b} \right)^2 \tag{3}$$

The drag coefficients in eqs 2 and 3 can be calculated from[15,16]

$$C_{Db} = C_{D0,b}(1 - f_b)^4 \tag{4}$$

where

$$C_{D0,b} = \frac{4}{3} \frac{g d_b}{{U_T}^2} \frac{\rho_l - \rho_g}{\rho_l} \tag{5}$$

$$U_T = \frac{\mu_l}{\rho_l d_b} M^{-0.149} (J - 0.857) \tag{6}$$

$$M = \frac{{\mu_l}^4 g (\rho_l - \rho_g)}{{\rho_l}^2 \sigma^3} \tag{7}$$

$$J = \begin{cases} 0.94 H^{0.757} & (2 < H \le 59.3) \\ 3.42 H^{0.441} & (H > 59.3) \end{cases} \tag{8}$$

$$H = \frac{4}{3} Eo \cdot M^{-0.149} \left(\frac{\mu_l}{\mu_{ref}} \right)^{-0.14} \tag{9}$$

$$Eo = \frac{g(\rho_l - \rho_g) {d_b}^2}{\sigma} \tag{10}$$

Then the total energy consumption N_T is resolved into three parts: the energy dissipation through the oscillation of bubble surfaces N_{surf}, the viscous energy dissipation in liquid N_{turb}, and the energy consumption for bubble breakage N_{break}. To close the model, a stability condition is proposed as the minimization of the microscale energy dissipation:

$$N_{surf} + N_{turb} = \min \tag{11}$$

With specified U_g, U_l, and physical properties of gas and liquid for the system, eqs 1−3 can be solved to obtain the structure variables f_S, f_L, and $U_{g,L}$ by giving the trial value for d_S, d_L, and $U_{g,S}$. Note that N_{surf}, N_{turb}, and N_{break} can be formulated as functions of structural parameters under specified U_g, U_l, and physical properties. So, the final solutions of the six structure parameters can be determined by the stability condition, i.e., eq 11. The details of this model can be referred to our previous publication.[13,14]

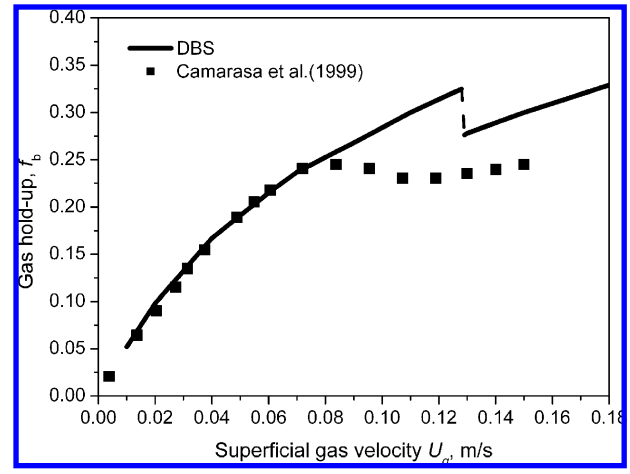

Figure 1. Comparison of gas hold-up between the DBS model and experiments of Camarasa et al.[4] with a multiple orifice nozzle, adapted from the work of Yang et al.[13]

Figure 1 indicates the jump change for gas hold-up at U_g = 0.128 m/s calculated in our previous work,[13] reflecting the second regime transition point reported by Camarasa et al.[4] Indeed, the jump change results from the switch of the global minimum point between two points with local minima of the stability criterion $(N_{surf} + N_{turb})/N_T$ in the solution space of structural parameters. This switch leads to the jump change of structural parameters and therefore the second transition point on gas hold-up curve. Further analysis shows that the local minimum point with larger value generates a pseudo solution of structure parameters when U_g is greater than 0.08 m/s, as depicted by the dash lines in Figure 2. The real solutions of gas hold-up and corresponding energy dissipation $(N_{surf} + N_{turb})/N_T$ at different gas velocities are plotted with solid lines. Apparently there are two branches in Figure 2: the energy dissipation curve of 1−1 corresponds to the hold-up curve 1′−1′, and the other branch 2−2, to the hold-up curve 2′−2′. The intersection of the two energy dissipation branches marks clearly the second regime transition point.

The transition from homogeneous and transition regimes to the fully developed heterogeneous regime can be physically understood from this intersection and bifurcation of the two curves. Each branch may represent a dominant mechanism, and the structure variation and the regime transition of system is essentially attributed to the competition between these two dominant mechanisms: at lower gas velocities, there exists only one local minimum corresponding to the initial segments of lines 1−1 and 1′−1′, and actually, small bubbles of similar size prevail in homogeneous regime. At intermediate velocities, the

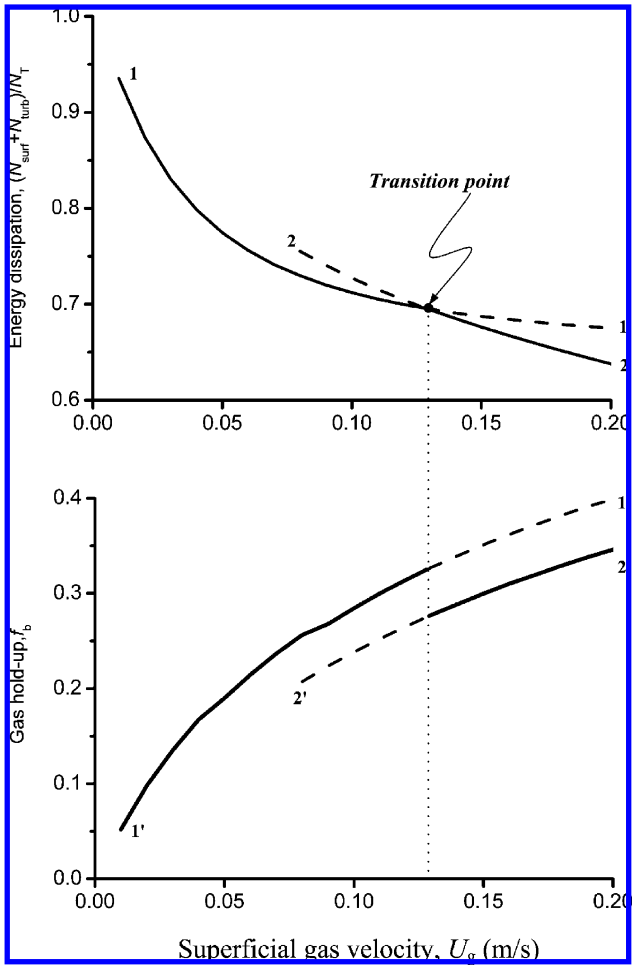

Figure 2. Relationship between structural bifurcation and energy dissipation in bubble columns.

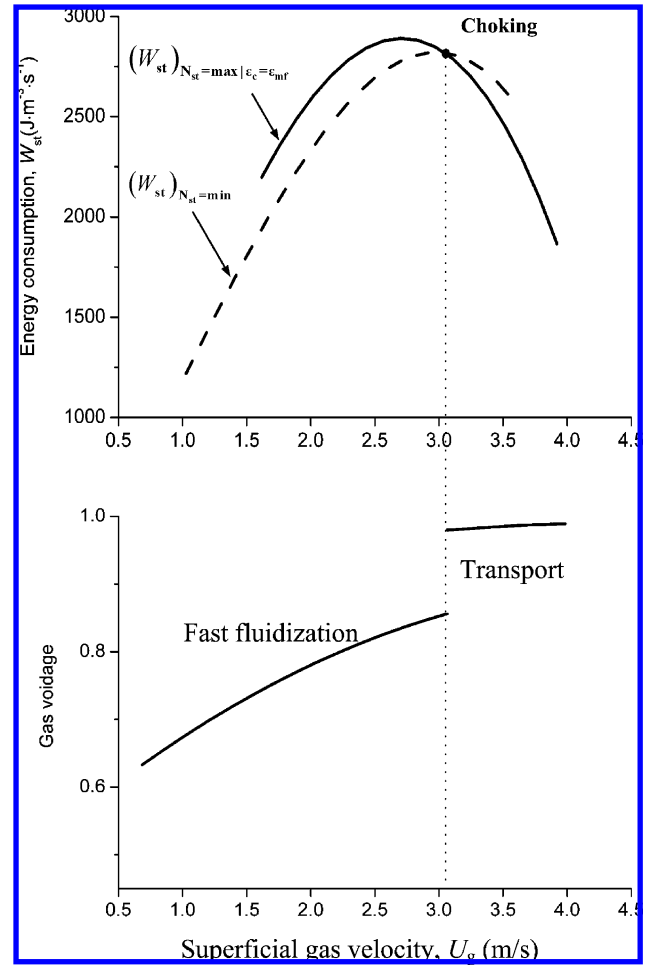

Figure 3. Mechanism of choking, adapted from the work of Li and Kwauk.[26]

other local minimum appears, denoted by the lines 2−2 and 2′−2′. This implies that another dominant mechanism starts to play its role in pattern formation, and in reality, large bubbles appear in the system due to bubble coalescence in the transition regime. But in this case, line 1−1 is still below line 2−2, and therefore, the system is still dominated by the first mechanism. With further increasing gas velocity, line 2−2 drops below line 1−1 and the second mechanism will take over the first one as the preferred mode of the system. The gas−liquid system in this case is in fully developed heterogeneous state with bubbles of wider size distribution.

This bifurcation phenomenon is similar to the previous calculation of Li et al.[17] on gas−solid fluidization with the energy-minimization multiscale (EMMS) model. Li et al.[17] postulated that the energy consumption for suspending and transporting particles per unit mass N_{st} tends to its minimum for dense fluidization in which particles and fluids have to compromise with each other, whereas it approaches maximum for dilute transport where fluid can dominate the two-phase system. Then, a critical condition was established to capture the so-called choking which marks the regime transition between dilute transport and dense fluidization, as shown in Figure 3. W_{st} denotes the energy consumption for suspending and transporting particles per unit volume. The choking point can be identified by the intersection of the two energy consumption branches. Ge and Li[18] further improved this model by employing N_{st} = min as a unified stability condition for all the regimes, and choking can be identified as a jump between two branches of the stable solution. The similarity in the bifurcation of energy dissipation between gas−liquid and gas−solid systems may be of significance for understanding the physical essence of structure evolution and regime transition of multiphase flow, and its theoretical basis and implication deserves further investigation and extension.

3. CFD Simulation Coupling with the DBS Model

3.1. Conservation Equations. Since the structure variation of global system can be reasonably predicted with the DBS model, we attempt to establish a relationship between gas−liquid interaction and structural parameters with this model and, then, incorporate it into a CFD simulation for the system of Camarasa et al.[4] with the commercial code Fluent 6.3.

Both the continuous liquid and dispersed bubble phases are modeled with an Eulerian approach as interpenetrating continua, and conservation equations for mass and momentum can be given by[19]

$$\frac{\partial \alpha_k}{\partial t} + \nabla\cdot(\alpha_k \mathbf{u}_k) = 0 \tag{12}$$

and

$$\frac{\partial \alpha_k \rho_k \mathbf{u}_k}{\partial t} + \nabla\cdot(\alpha_k \rho_k \mathbf{u}_k \mathbf{u}_k) = -\alpha_k \nabla P + \alpha_k \rho_k g \pm \mathbf{F}_{kl} + \nabla\cdot(\alpha_k \tau_k) + \nabla\cdot(\alpha_k \rho_k \mathbf{u}_k' \mathbf{u}_k') \tag{13}$$

where $\mathbf{F}_{kl}$ is the interphase momentum exchange term. The viscous stress tensor τ_k can be expressed by

$$\tau_k = \mu_k(\nabla \mathbf{u}_k + \nabla \mathbf{u}_k^{\mathrm{T}}) - \frac{2}{3}\mu_k \nabla \cdot \mathbf{u}_k \mathbf{I} \quad (14)$$

The term $\alpha_k \rho_k \mathbf{u}_k' \mathbf{u}_k'$ in eq 13 denotes the turbulent stress tensor and is modeled by the standard $k-\varepsilon$ model for the liquid phase and the Tchen turbulence model for gas.[20] Detail of the models can be referred to FLUENT software manual.

3.2. Interphase Coupling. Interphase coupling is still a great challenge for CFD simulation of multiphase flow, and generally, only drag force is taken into account and other forces like lift and virtual mass force can be omitted. Therefore, the interphase momentum transfer is modeled only through the drag force:

$$\mathbf{F}_{\mathrm{lg}}^{\mathrm{D}} = \frac{3}{4}\alpha_{\mathrm{g}}\frac{C_{\mathrm{D}}}{d_{\mathrm{b}}}\rho_{\mathrm{l}}|\mathbf{u}_{\mathrm{l}} - \mathbf{u}_{\mathrm{g}}|(\mathbf{u}_{\mathrm{l}} - \mathbf{u}_{\mathrm{g}}) \quad (15)$$

Here the effective drag coefficient C_{D} for a bubble immersed in a liquid with bubble swarms can be obtained by correcting C_{D0} for a bubble in the absence of other bubbles with an exponential function of liquid volume fraction α_{l} or simply multiplying α_{l}. C_{D0} can be either calculated from correlations of terminal velocity[15,21,22] or formulated directly as functions of Reynolds number *Re*, Eötvos number *Eo* (the ratio of gravity to surface tension), or Morton number with consideration of liquid properties. To avoid the volume fraction dependent drag coefficient, another way demonstrated in the literature is to only employ the correlation for C_{D0} for interphase coupling but to adjust the bubble diameter in eq 15. Note that we employed eq 4 to calculate C_{D} in the DBS model.

Since C_{D} is affected by the correction function for volume fraction and d_{b} represents an averaged value of the wide bubble size distribution, both of which involve some uncertainty, and thus $(C_{\mathrm{D}}/d_{\mathrm{b}})$ in eq 15 plays an essential role in CFD simulation. Thakre and Joshi[23] estimated drag force with

$$\mathbf{F}_{\mathrm{lg}}^{\mathrm{D}} = \alpha_{\mathrm{g}}(\rho_{\mathrm{l}} - \rho_{\mathrm{g}})g(\mathbf{u}_{\mathrm{l}} - \mathbf{u}_{\mathrm{g}})/\overline{(\mathbf{u}_{\mathrm{l}} - \mathbf{u}_{\mathrm{g}})} \quad (16)$$

where $\overline{(\mathbf{u}_{\mathrm{l}} - \mathbf{u}_{\mathrm{g}})}$ was set as a constant average slip velocity (0.2 m/s) for air−water systems. Similarly, $(C_{\mathrm{D}}/d_{\mathrm{b}})$ was set as 290 m^{-1} by Ranade.[24]

In this work, the drag force for each bubble class in unit volume can be calculated from eqs 2 and 3 of the DBS model since all the six structure variables of the two bubble classes have already been obtained. The total drag force can be expressed as:

$$F_{\mathrm{D}} = f_{\mathrm{S}}\rho_{\mathrm{l}}g + f_{\mathrm{L}}\rho_{\mathrm{l}}g \quad (17)$$

Considering the force balance for one single equivalent bubble phase, we obtain

$$F_{\mathrm{D}} = \frac{f_{\mathrm{b}}}{\pi/6 \cdot d_{\mathrm{b}}^{3}} \cdot C_{\mathrm{D}}\frac{\pi}{4}d_{\mathrm{b}}^{2} \cdot \frac{1}{2}\rho_{\mathrm{l}}\left(\frac{U_{\mathrm{g}}}{f_{\mathrm{b}}} - \frac{U_{\mathrm{l}}}{1 - f_{\mathrm{b}}}\right)^2 \quad (18)$$

For semibatch mode in bubble columns where $U_{\mathrm{l}} = 0$, combination of eqs 2, 3, 17, and 18 leads to

$$\frac{f_{\mathrm{b}}}{d_{\mathrm{b}}} \cdot C_{\mathrm{D}}\left(\frac{U_{\mathrm{g}}}{f_{\mathrm{b}}}\right)^2 = \frac{f_{\mathrm{S}}}{d_{\mathrm{S}}} \cdot C_{\mathrm{D,S}}\left(\frac{U_{\mathrm{g,S}}}{f_{\mathrm{S}}}\right)^2 + \frac{f_{\mathrm{L}}}{d_{\mathrm{L}}} \cdot C_{\mathrm{D,L}}\left(\frac{U_{\mathrm{g,L}}}{f_{\mathrm{L}}}\right)^2 \quad (19)$$

Finally the ratio of drag coefficient to the bubble diameter for the equivalent bubble phase can be formulated as

$$\frac{C_{\mathrm{D}}}{d_{\mathrm{b}}} = \left[\frac{f_{\mathrm{S}}}{d_{\mathrm{S}}} \cdot C_{\mathrm{D,S}}\left(\frac{U_{\mathrm{g,S}}}{f_{\mathrm{S}}}\right)^2 + \frac{f_{\mathrm{L}}}{d_{\mathrm{L}}} \cdot C_{\mathrm{D,L}}\left(\frac{U_{\mathrm{g,L}}}{f_{\mathrm{L}}}\right)^2\right]\frac{f_{\mathrm{b}}}{U_{\mathrm{g}}^{2}} \quad (20)$$

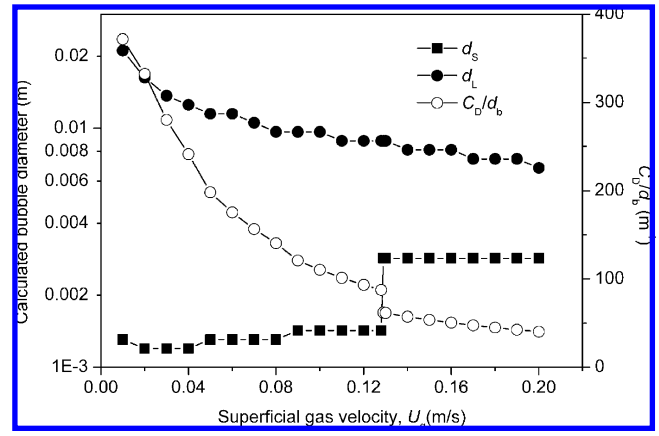

Figure 4. Bubble diameters and the ratio of drag coefficient to bubble diameter obtained from the DBS model.

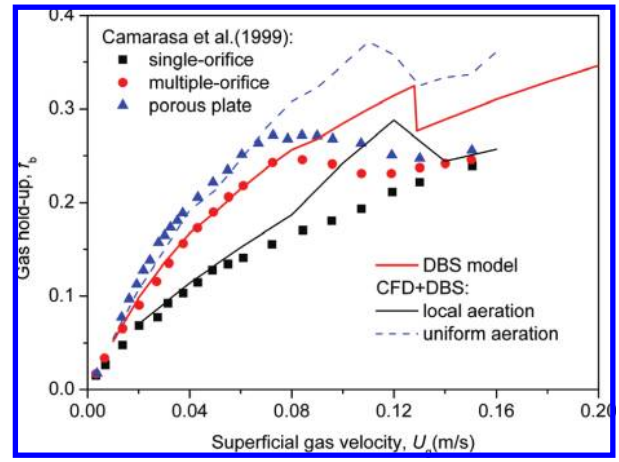

Figure 5. Variation of gas hold-up curve with superficial gas velocity: CFD results vs experimental results in the literature.[4]

It can be seen that $C_{\mathrm{D}}/d_{\mathrm{b}}$ is a function of superficial gas velocity and structural parameters of the two bubble classes. Figure 4 illustrates the variation of $C_{\mathrm{D}}/d_{\mathrm{b}}$ with U_{g}. The coupling between the DBS model and two-fluid model can be implemented by substituting eq 20 into eq 15 to calculate the interphase momentum exchange. It should be pointed out that d_{S} and d_{L} shown in Figure 4 can only be understood as intermediate parameters for calculating drag force, rather than represent the real values of bubble diameters because their magnitude is also dependent on the correlations for standard drag coefficient C_{D0} and correction factor for gas volume fraction. Thus, only the ratio of $C_{\mathrm{D}}/d_{\mathrm{b}}$ or the drag force is meaningful in this context of CFD simulation.

3.3. Initial and Boundary Conditions. The bubble column of Camarasa et al.[4] and Olmos et al.[9] with an inside diameter of 10 cm and a height of 2 m is simulated with the aforementioned model. Spargers in these experiments were either single-orifice, multiorifice, or porous plate which increases the aeration uniformity in turn. Superficial gas velocity varies from 0.01 to 0.16 m/s. Initially, the column is filled with liquid up to a static height of 1.0 m. Gas fills the top zone as a gas cap ($\alpha_{\mathrm{g}} = 1$; $\alpha_{\mathrm{l}} = 0$). To investigate the influence of different aeration ways, two inlet conditions are configured in the 2D simulation. In the "uniform aeration" case, the whole plane at the bottom of the column is aerated, but for the "local aeration" case, only the central 40% of bottom is allowed to aerate. The grid size is 5 mm × 5 mm for the uniform aeration and 2.5 mm × 10 mm for the local aeration in the 2D unsteady simulation. Of course,

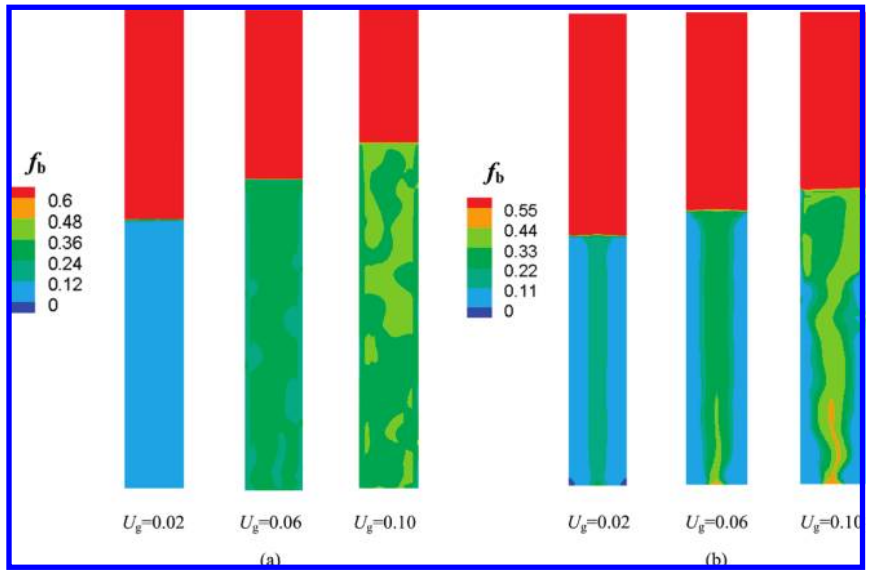

Figure 6. Maps of gas hold-up: (a) uniform aeration; (b) local aeration.

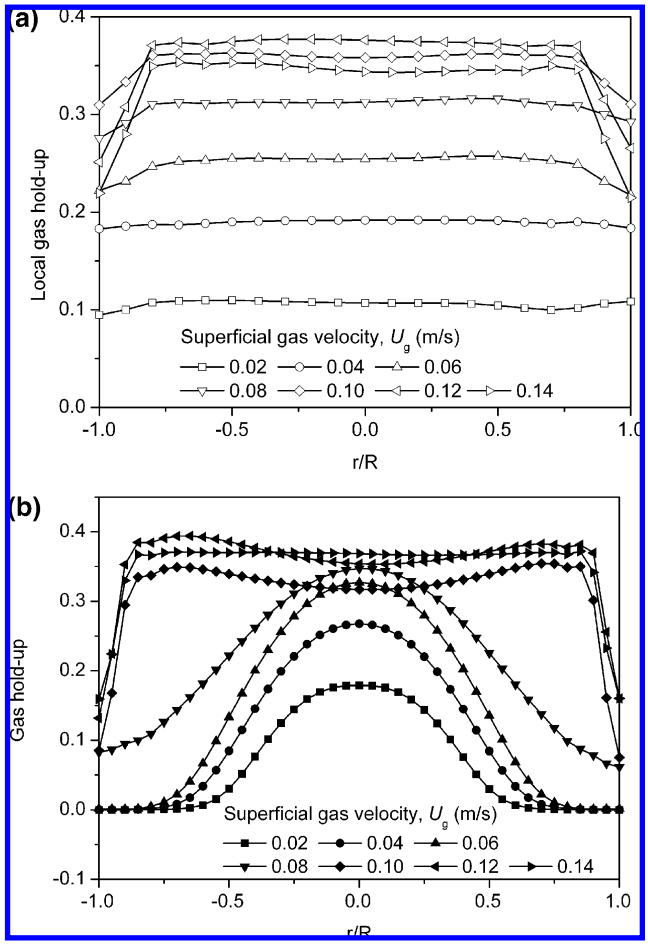

Figure 7. Radial distribution of simulated local gas hold-up for different superficial gas velocities: (a) uniform aeration; (b) local aeration.

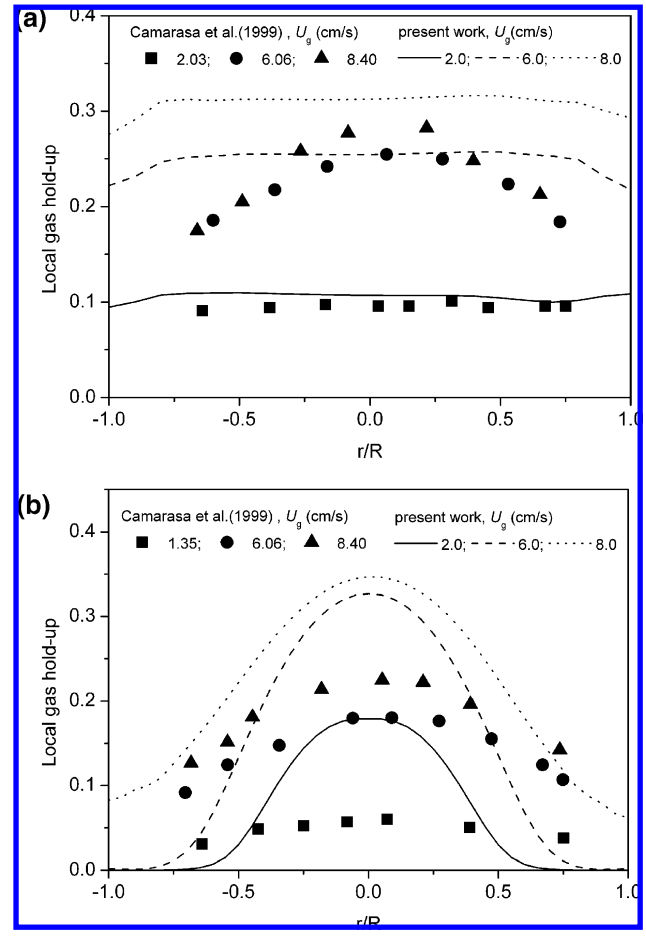

Figure 8. (a) Simulation of uniform aeration vs experimental data of a porous plate sparger. (b) Simulation of local aeration vs experimental data of a single-orifice sparger.

these configurations in the 2D simulation cannot represent the real sparger types but may be used as a first approximation to study the influence of various aeration ways with an acceptable computational cost. The so-called pressure outlet boundary condition is applied for the top outlet with the backflow volume fraction of gas being 1. For both phases, nonslip boundary conditions are employed for the confining solid walls. Serious numerical problems may be caused by the large volume fraction gradient at the gas−liquid interface and high gas volume fraction in the cap. This problem is avoided by special treatment of drag coefficient suggested by Zhang et al.[25] that C_D is set as 0.05 when α_l is less than 0.55. A first-order upwind discretization scheme is used for the solution of model equations and the convergence criteria are set to be 10^{-3}. The time step is fixed to be 0.005 s in all calculations and quasi-steady state is

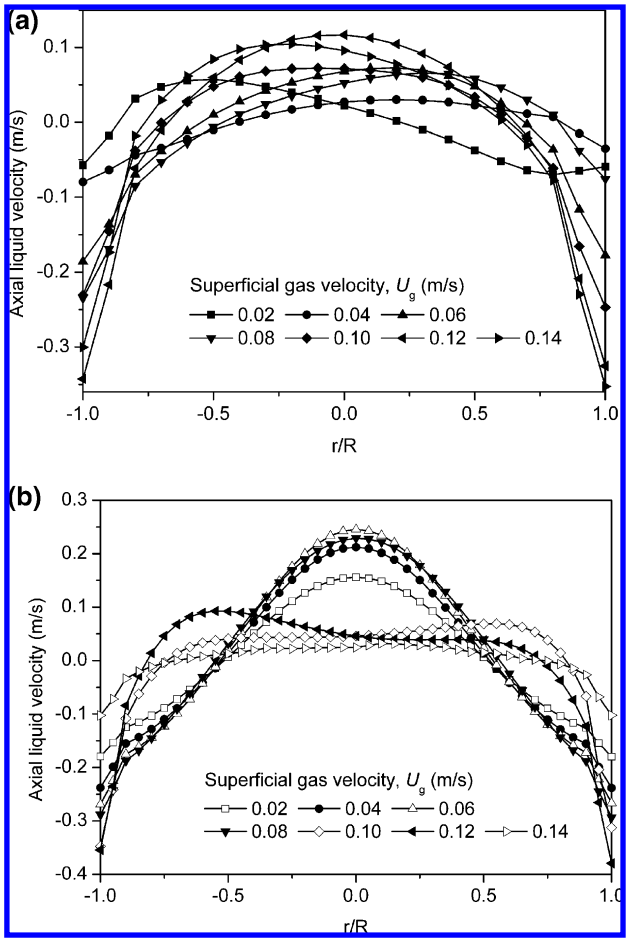

Figure 9. Radial distribution of simulated axial liquid velocity for different superficial gas velocities: (a) uniform aeration; (b) local aeration.

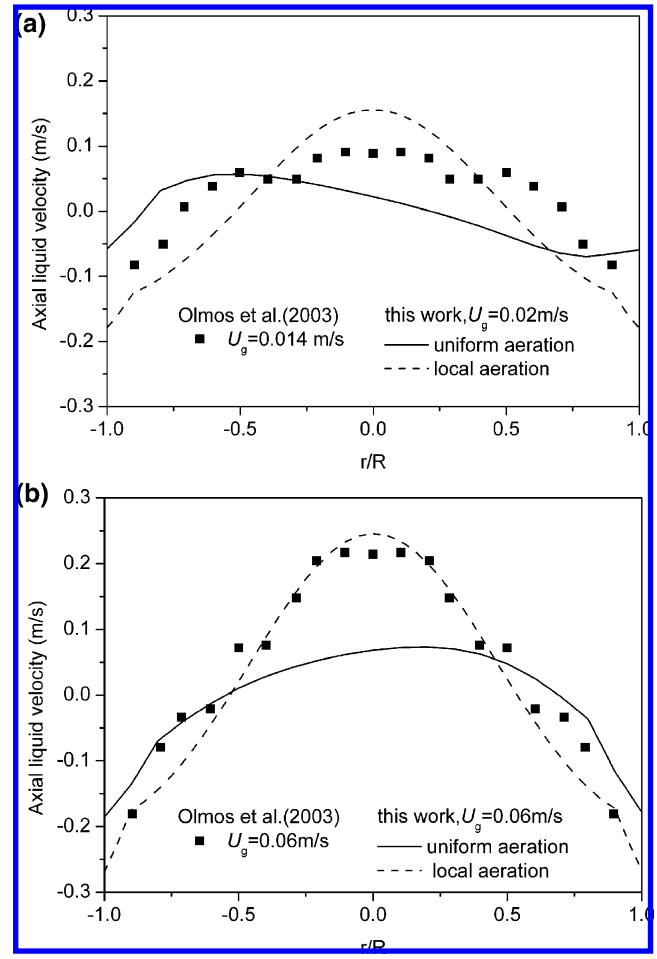

Figure 10. Comparison of axial liquid velocity between the simulation and experimental data of Olmos et al.:[9] U_g = (a) 0.02 and (b) 0.06 m/s.

considered to achieve in 100 s, and then, the time-averaged quantities are obtained by averaging the instantaneous values in the next 100 s.

3.4. Results and Discussion. Figure 5 compares the simulation of total gas hold-up with experimental data of Camarasa et al.[4] In their experiments, the single-orifice nozzle was 5 mm in diameter for local aeration and the multiple-orifice-nozzle was composed of 62 holes of 1 mm uniformly spaced. The porous glass plate was 5 mm in height with 10−16 μm mean pore diameter for uniform aeration.

For the different sparger types of single-orifice nozzle, multiple-orifice-nozzle, and porous plate, the measured total gas hold-up increases in turn, as shown in Figure 5. The simulated total gas hold-up is higher in the uniform case than that in the local aeration case, which is consistent with the experimental trends. This is pertinent to the size of bubbles produced from different spargers: the fine pore of porous plate generates smaller bubbles which may not be coalesced at lower and intermediate flow rates.

For the uniform aeration case, the experimental finding on the second transition point at $U_g > 0.12$ m/s of Zahradnik et al.[2] can be reproduced by the DBS model and the CFD simulation in this work. For the uniform aeration case, the total gas hold-up first decreases between 0.11 and 0.13 m/s and then increases again. This turnover on the gas hold-up curve is related to the drag model proposed in this work. It can be seen from Figure 4 that C_D/d_b drops at the second transition point, leading to a weaker interphase interaction. So the gas phase can pass through the liquid bulk more quickly and thus causes a lower hold-up.

The CFD simulation for the local aeration case also exhibits a transition, but the experimental data shows a monotonous increase for single-orifice aeration. This deviation may be attributed to the interphase coupling method. Because C_D/d_b as a function of U_g calculated by the DBS model is adopted in both the uniform and local aeration cases, so the jump change in C_D/d_b as shown in Figure 4 is responsible for the false transition in the local aeration case.

Current simulation shows obvious deviation of the total gas hold-up for both uniform and local aeration cases from the experimental data for higher gas velocities. The deviation may come from two aspects: first the 2D simulation is not enough to depict the configuration of real spargers; second, the DBS model itself overpredicts the total gas holdup than the experimental data for higher gas velocities, as shown in Figure 1. The DBS model does not consider the gas ejection, boundary conditions, and the contamination of the experimental media which may promote or inhibit the bubble coalescence.

Figure 6 shows the contour plots of gas hold-up for three superficial gas velocities 0.02, 0.06, and 0.10 m/s. All the instantaneous snapshots are taken at 200s when the quasi-steady state is attained. For the uniform aeration case as shown in Figure 6a, the homogeneous regime is observed at $U_g = 0.02$ m/s. The gas holdup for 0.06 and 0.10 m/s takes on a nearly homogeneous profile with some local heterogeneity. However, for the local aeration case as shown in Figure 6b, the heterogeneous structure is always observed even for $U_g = 0.02$ m/s. The central gas jet drifts liquid upward and causes an intense liquid back-mixing at the two sides of the bubble column

for the local aeration case. For the uniform aeration case, the flow structure is dependent on the inherent hydrodynamic stability of gas−liquid two phase flow. In other words, the flow regime evolves from homogeneous to heterogeneous due to the inherent flow instability. On the other hand, local aeration produces instability at the inlet boundary, leading to the onset of heterogeneous regime at lower gas velocities. This difference has been reported by Ruzicka et al.,[5] and the so-called THeR (heterogeneous regime resulted from the instability of the homogeneous regime) and PHeR (pure heterogeneous regime) were differentiated.

Figures 7−9 illustrate the radial distribution of gas hold-up and axial liquid velocities for the both aeration cases. The radial distribution is obtained by averaging instantaneous quantities in 100 s. All the profiles except the uniform cases of $U_g = 0.12$ and 0.14 m/s are plotted for the plane of 1.0 m of column height, and in the latter two cases, data for 0.5 m of column height is drawn as the steady liquid interface is below 1.0 m due to strong liquid entrainment.

Figure 7a shows the simulated radial distribution of local gas hold-up at different U_g for uniform aeration. It can be seen that a uniform profile is obtained for lower gas velocities, corresponding to the homogeneous regime. For the transition and heterogeneous regime a flat distribution appears in the center and a sharp drop near the wall. For the local aeration case shown in Figure 7b, parabolic profiles can be observed for U_g less than 0.08 m/s. Similar to the uniform aeration case, a central flat profile with a sharp drop near the wall is obtained for higher gas velocities of local aeration case.

The simulation for uniform aeration case is fairly consistent with the experimental data of porous plate for low gas velocity, as shown in Figure 8a, but it deviates from the experimental parabolic profile at intermediate gas velocity. This may arise from the difference between the ideal uniform aeration in the 2D simulation and nonideal aeration of porous plates in experiments. The influence of this difference may be minor for low velocities but becomes apparent for intermediate and high velocities. In contrast, the 2D simulation with local aeration can produce the parabolic distribution, as shown in Figure 8b.

Figure 9 illustrates the simulated radial distribution of axial liquid velocity for different U_g. The local aeration produces steeper distribution than the uniform aeration for $U_g < 0.10$ m/s. For higher gas velocities, a slight saddle profile is found in the local aeration case. The change from parabolic to saddle profile is related to the expansion of central bubble plume shown in Figure 6b. The plume disperses to almost the whole section at the height of 1.0 m for higher gas velocities. Figure 10 illustrates the comparison of simulation and available experimental data for the cases of porous plate and multiple-orifice spargers.[9] The local aeration case is close to the experiment data but the uniform aeration case shows serious deviation.

4. Conclusions

The second regime transition point can be captured as a jump change of gas hold-up by the dual-bubble-size (DBS) model. Physically this can be understood through the bifurcation of microscale energy dissipation between two branches. The bifurcation which was first explored in the EMMS model of our previous work to predict the so-called choking in gas−solid fluidization can also find its counterpart in gas−liquid systems in this work. Each branch may represent a candidate of stable state, and the switch from one to the other signifies the fundamental variation of system structure leading to the regime transition. The ratio of drag coefficient to the bubble diameter C_D/d_b is of critical importance for CFD simulation and can be obtained by the DBS model calculation. CFD simulation incorporating the DBS model for interphase coupling can reproduce the shoulder and the second transition point on the gas hold-up curve. Sparger effects are conceptually investigated by imposing different aeration in the 2D simulation. It is found that uniform aeration can generate a larger total gas hold-up than local aeration.

Acknowledgment

The authors wish to thank the National Natural Science Foundation of China for the long term financial support under grants 20406022, 20221603, and 20490201 and from the National Basic Research Program of China under the grant 2009CB219906.

Nomenclature

C_{Db} = drag coefficient for a bubble in a swarm, dimensionless
$C_{D0,b}$ = drag coefficient for a bubble in a quiescent liquid, dimensionless
C_{Dp} = drag coefficient for a particle in multiparticle systems, dimensionless
$C_{D0,p}$ = drag coefficient for a particle in a quiescent fluid, dimensionless
d_b = bubble diameter, m
d_L = bubble diameter of large bubbles, m
d_S = bubble diameter of small bubbles, m
Eo = Eötvos number, dimensionless
f_b = volume fraction of gas phase, dimensionless
f_L = volume fraction of large bubbles, dimensionless
f_S = volume fraction of small bubbles, dimensionless
g = gravitational acceleration, m/s^2
Mo = Morton number, dimensionless
N_{break} = rate of energy consumption due to bubble breakage and coalescence per unit mass, m^2/s^3
N_{surf} = rate of energy dissipation due to bubble oscillation per unit mass, m^2/s^3
N_{turb} = rate of energy dissipation in turbulent liquid phase per unit mass, m^2/s^3
N_{st} = rate of energy dissipation for suspending and transporting particles per unit mass, m^2/s^3
U_g = superficial gas velocity, m/s
$U_{g,L}$ = superficial gas velocity for large bubbles, m/s
$U_{g,S}$ = superficial gas velocity for small bubbles, m/s
U_l = superficial liquid velocity, m/s
W_{st} = rate of energy dissipation for suspending and transporting particles per unit volume, J/(m^3 s)

Greek Letters

α = void fraction, dimensionless
ε = voidage, dimensionless
μ = viscosity, Pa·s
ρ = density, kg/m^3
σ = surface tension, N/m
τ = shear stress tensor
ω = collision frequency, 1/s

Abbreviations

DBS = double-bubble-size
EMMS = energy-minimization multiscale
PHeR = pure heterogeneous regime
SBS = single-bubble-size
THeR = heterogeneous regime resulted from the instability of homogeneous regime

Subscripts
g = gas
k = phase index
l = liquid
L = large bubble
p = particle
S = small bubble

Literature Cited

(1) Shaikh, A.; Al-Dahhan, M. H. A Review on Flow Regime Transition in Bubble Columns. *Int. J. Chem. React. Eng.* **2007**, *57*, 1–68.

(2) Zahradnik, J.; Fialova, M.; Ruzicka, M.; Drahos, J.; Kastanek, F.; Thomas, N. H. Duality of the gas-liquid flow regimes in bubble column reactors. *Chem. Eng. Sci.* **1997**, *52*, 3811–3826.

(3) Chen, R. C.; Reese, J.; Fan, L.-S. Flow structure in a three-dimensional bubble column and three-phase fluidized bed. *AIChE J.* **1994**, *40*, 1093–1104.

(4) Camarasa, E.; Vial, C.; Poncin, S.; Wild, G.; Midoux, N.; Bouillard, J. Influence of coalescence behaviour of the liquid and of gas sparging on hydrodynamics and bubble characteristics in a bubble column. *Chem. Eng. Process.* **1999**, *38*, 329–344.

(5) Ruzicka, M. C.; Zahradnik, J.; Drahos, J.; Thomas, N. H. Homogeneous-heterogeneous regime transition in bubble columns. *Chem. Eng. Sci.* **2001**, *56*, 4609–4626.

(6) Zuber, N.; Findlay, J. A. Average volumetric concentration in two-phase flow systems. *Int. J. Heat Transfer* **1965**, *87*, 453–468.

(7) Joshi, J. B.; Deshpande, N. S.; Dinkar, M.; Phanikumar, D. V. Hydrodynamic stability of multiphase reactors. In *Advances in Chemical Engineering*; Academic Press: New York, 2001; Vol. 26, pp 1−130.

(8) Krishna, R.; Urseanu, M. I.; van Baten, J. M.; Ellenberger, J. Influence of scale on the hydrodynamics of bubble columns operating in the churn-turbulent regime: experiments vs. Eulerian simulations. *Chem. Eng. Sci.* **1999**, *54*, 4903–4911.

(9) Olmos, E.; Gentric, C.; Midoux, N. Numerical description of flow regime transitions in bubble column reactors by a multiple gas phase model. *Chem. Eng. Sci.* **2003**, *58*, 2113–2121.

(10) Monahan, S. M.; Vitankar, V. S.; Fox, R. O. CFD predictions for flow-regime transitions in bubble columns. *AIChE J.* **2005**, *51*, 1897–1923.

(11) Wang, T.; Wang, J.; Jin, Y. Theoretical prediction of flow regime transition in bubble columns by the population balance model. *Chem. Eng. Sci.* **2005**, *60*, 6199–6209.

(12) Simonnet, M.; Gentric, C.; Olmos, E.; Midoux, N. CFD simulation of the flow field in a bubble column reactor: Importance of the drag force formulation to describe regime transitions. *Chem. Eng. Process.* **2008**, *47*, 1726–1737.

(13) Yang, N.; Chen, J.; Zhao, H.; Ge, W.; Li, J. Explorations on the multi-scale flow structure and stability condition in bubble columns. *Chem. Eng. Sci.* **2007**, *62*, 6978–6991.

(14) Chen, J.; Yang, N.; Ge, W.; Li, J. Modeling of Regime Transition in Bubble Columns with Stability Condition. *Ind. Eng. Chem. Res.* **2009**, *48*, 290–301.

(15) Grace, J. R.; Wairegi, T.; Nguyen, T. H. Shapes and velocities of single drops and bubbles moving freely through immiscible liquids. *Trans. Inst. Chem. Eng.* **1976**, *54*, 167–173.

(16) Clift, R.; Grace, J. R.; Weber, M. E. *Bubbles, Drops, and Particles*; Academic Press: London, 1978.

(17) Li, J.; Cheng, C.; Zhang, Z.; Yuan, J.; Nemet, A.; Fett, F. N. The EMMS model -- its application, development and updated concepts. *Chem. Eng. Sci.* **1999**, *54*, 5409–5425.

(18) Ge, W.; Li, J. Physical mapping of fluidization regimes--the EMMS approach. *Chem. Eng. Sci.* **2002**, *57*, 3993–4004.

(19) Chen, P.; Dudukovic, M. P.; Sanyal, J. Three-dimensional simulation of bubble column flows with bubble coalescence and breakup. *AIChE J.* **2005**, *51*, 696–712.

(20) Hinze, J. O. *Turbulence*. McGraw-Hill Publishing Co.: New York, 1975.

(21) Fan, L.-S.; Tsuchiya, K. *Bubble wake dynamics in liquids and liquid-solid suspensions*. Butterworth-Heinemann: Stoneham, 1990.

(22) Krishna, R.; Ellenberger, J. Gas holdup in bubble column reactors operating in the churn-turbulent flow regime. *AIChE J.* **1996**, *42*, 2627–2634.

(23) Thakre, S. S.; Joshi, J. B. CFD simulation of bubble column reactors: importance of drag force formulation. *Chem. Eng. Sci.* **1999**, *54*, 5055–5060.

(24) Ranade, V. V. Modeling of turbulence flow in a bubble column reactor. *Chem. Eng. Res. Des.* **1997**, *75*, 14–23.

(25) Zhang, D.; Deen, N. G.; Kuipers, J. A. M. Euler-Euler Modeling of Flow, Mass Transfer, and Chemical Reaction in a Bubble Column. *Ind. Eng. Chem. Res.* **2009**, *48*, 47–57.

(26) Li, J.; Kwauk, M. *Particle-Fluid Two-Phase Flow-The Energy-Minimization Multi-Scale Method*.; Metallurgical Industry Press: Beijing, 1994.

Received for review October 28, 2008
Revised manuscript received April 30, 2009
Accepted May 4, 2009

IE801644D